

Article

Delivery of cations (Mg^{2+} , Al^{3+} , Ga^{3+} , Sn^{2+} , Cr^{3+} , Fe^{3+}) into the cells by anthocyanins through Physico-chemical assessment: A molecular simulation study

Fatemeh Mollaamin^{1,*}, Majid Monajjemi²¹ Department of Biomedical Engineering, Faculty of Engineering and Architecture, Kastamonu University, Kastamonu 37150, Turkey² Department of Chemical Engineering, Central Tehran Branch, Islamic Azad University, Tehran 1496969191, Iran* **Corresponding author:** Fatemeh Mollaamin, fmollaamin@kastamonu.edu.tr, smollaamin@gmail.com

CITATION

Mollaamin F, Monajjemi M. Delivery of cations (Mg^{2+} , Al^{3+} , Ga^{3+} , Sn^{2+} , Cr^{3+} , Fe^{3+}) into the cells by anthocyanins through Physico-chemical assessment: A molecular simulation study. *Molecular & Cellular Biomechanics*. 2024; 21(2): 206.
<https://doi.org/10.62617/mcb.v21i2.206>

ARTICLE INFO

Received: 21 June 2024

Accepted: 23 August 2024

Available online: 5 November 2024

COPYRIGHT



Copyright © 2024 by author(s).
Molecular & Cellular Biomechanics is published by Sin-Chn Scientific Press Pte. Ltd. This work is licensed under the Creative Commons Attribution (CC BY) license.
<https://creativecommons.org/licenses/by/4.0/>

Abstract: Anthocyanins (ACNs) are secondary metabolites responsible for most of the red to purple pigmentation found in flowers, fruits, and leaves. Clusters of metal ions of Mg^{2+} , Al^{3+} , Ga^{3+} , Sn^{2+} , Cr^{3+} , Fe^{3+} joined to ACNs in water media were studied for unraveling the color shifting of different complexes of these structures in the low ranges of pH. In this verdict, it has been studied the metallic cations diffusing of deprotonating for the anthocyanin (ACN) (B)-ring of Malvidin (Mal), Peonidin (Peo), Delphinidin (Del), Pet, and Cyanidin (Cya) in water. The difference of heat of formation (ΔH_f) among clusters of metallic cations jointed to ACNs has been illustrated toward the double bonds and carbonyl groups by the chelation of (B)-ring for cyanidin, delphinidin and petunidin ACNs in two media of gas and water that explains the stability and color of [ACN-metallic cations] cluster chelation. The complexes of $Ga^{3+} \rightarrow$ Pet, $Cr^{3+} \rightarrow$ Pet, $Mg^{2+} \rightarrow$ Pet and $Al^{3+} \rightarrow$ Cya, $Ga^{3+} \rightarrow$ Cya, $Mg^{2+} \rightarrow$ Cya have indicated the maximum absorbance in the low concentration. The mechanism of cation-induced ACNs mainly depends on the location of active zones of functionalized O-atoms in ACN and divalent or trivalent cations characteristics. Regarding the obtained results, regular consumption of some vegetables and fruits, which are rich in ACN molecules, should be helpful to stop viral infectious by decreasing pathogenicity and propagation of viral diseases.

Keywords: fruits and vegetables; ACNs; cation metal chelation; water

1. Introduction

The dangerous viral malady in 2019 was new Coronavirus disease (COVID-19) which is known as severe acute respiratory syndrome (SARS-CoV-2) [1–6]. Natural drugs and herbs with their anti-inflammatory properties might have pleiotropic functions in COVID-19 treatment [7–11].

Some antibodies extracted from plants are supposed to answer very quickly to the emergence of recent variants of COVID-19 [12–19].

ACNs are one of the four subclasses of Flavonoids [20] which represent various beneficial impressions consisting of antidiabetes, anticancer, antiallergy, antimutagenesis, cardioprotection, and antiviral activities [21,22]. One of the beneficial methods for discovering proper medication against COVID-19 can be molecular docking approach. This method can analyze the conformation and orientation of molecular structures into the binding zones of a macromolecular object [23]. Many research works have been remarked on the application of molecular docking method to determine or foretell the drug-object binding tendency with the

viral protease [24–32]. The ACNs attached to some cations containing Mg^{2+} , Al^{3+} , Ga^{3+} , Sn^{2+} , Cr^{3+} , Fe^{3+} have been shown in **Figure 1**.

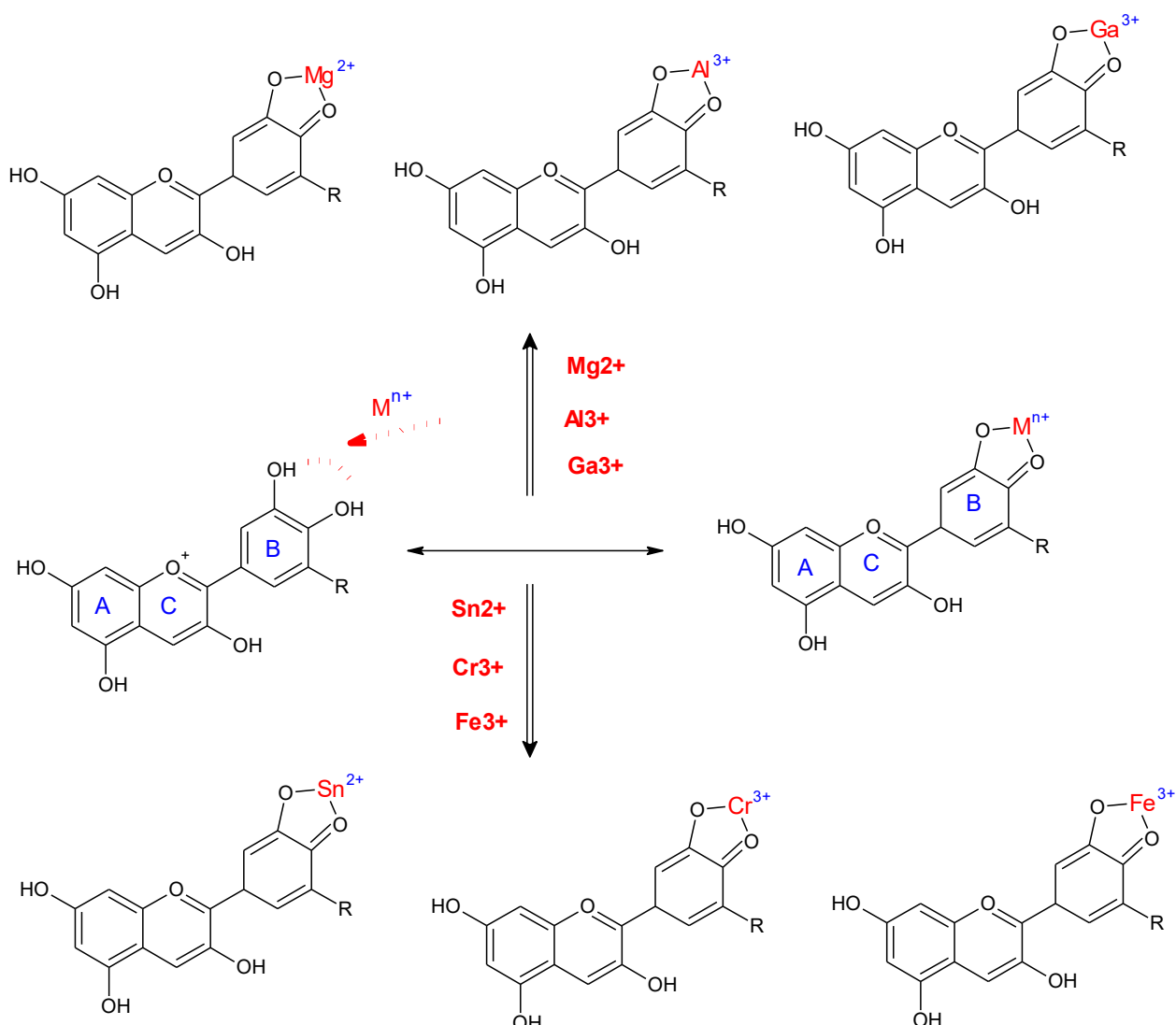
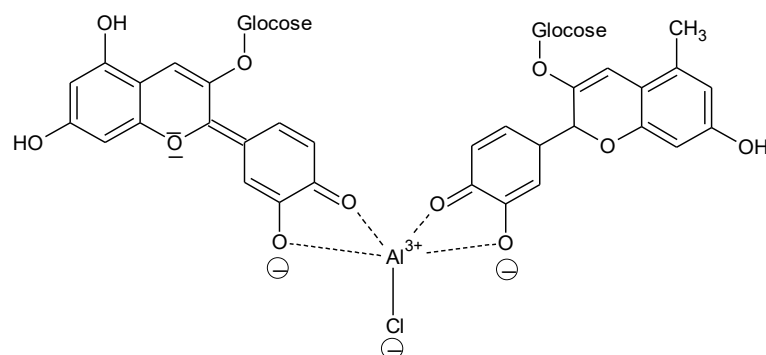


Figure 1. ACN is attached to some cations consisting of Mg^{2+} , Al^{3+} , Ga^{3+} , Sn^{2+} , Cr^{3+} , Fe^{3+} .

Free essential radicals are generated and twisted, for instance, in the defense against pathogenic bacteria and viruses. Antioxidants are extremely valuable food ingredients for our health [33–39]. For example, the chelation of Al^{3+} by ACNs was more investigated owing to its dependence. The complexes with acceptable stability between Del and Al were found (**Scheme 1**) [40].



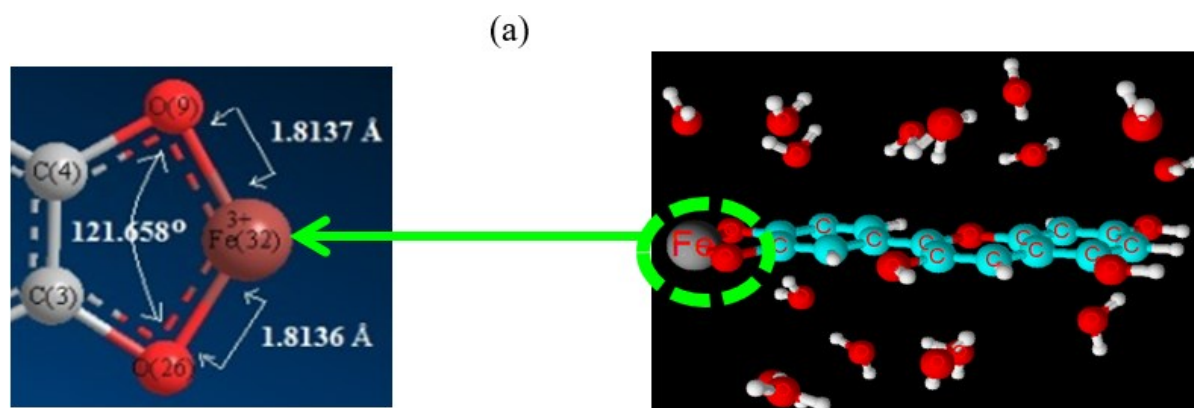
Scheme 1. Aluminum ion chelated with delphinidin-3-monoglucoside which reflects a blue light.

Del as its flavylum cation conducts red solutions in the model system. the Al³⁺ removes H⁺ ions from delphinidin, converting delphinidin's flavylum cation to its blue quinoidal base anion which complexes with the Al³⁺. Regarding the stability of this complex, a second flavylum cation accumulates on top of the complexed quinoidal base anion, generating a bathochromic shift of the cation's spectral effect and indicating the blue color [41].

Applying this approach, it can be remarked these dietary structures belong to the subclass of ACN, which demonstrate the main ingredients in vegetables and fruits, as rich inhibiting agents of the main protease and targeting the receptor-binding domain (RBD) of S-protein for SARS-CoV2. In addition, molecular docking assigns swift diagnosis of the amino acid sequences for SARS-CoV-2 [42–44]. ACNs are present in the highest concentration in some vegetables and fruits. The present investigation measures the ability of these compounds for inhibiting the main protease and the receptor-binding domain of spike glycoprotein of SARS-CoV-2 using mechanic quantum approaches.

2. Materials and methods

Geometry optimization of Mg²⁺ → Cya, Al³⁺ → Cya, Ga³⁺ → Cya, Sn²⁺ → Cya, Cr³⁺ → Cya, and Fe³⁺ → Cya chelation complexes through their B ring in water at 300K have been calculated using Gaussian 16 revision C.01 program [45]. In addition, the properties of Bader charge and thermodynamic parameters of Mg²⁺ → ACN, Al³⁺ → ACN, Ga³⁺ → ACN, Sn²⁺ → ACN, Cr³⁺ → ACN, and Fe³⁺ → ACN chelation through their B ring in aqueous medium at 300K have been computed (**Figure 2**).



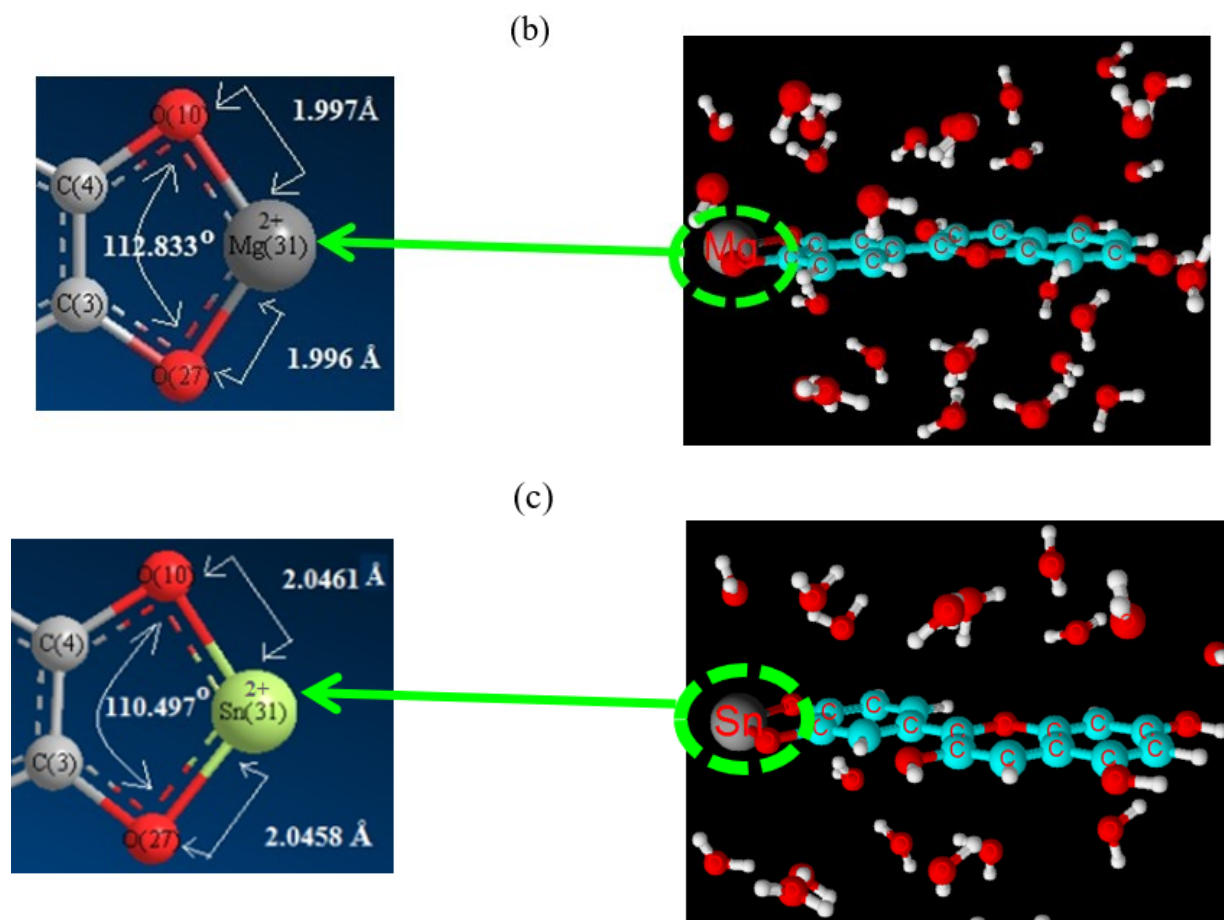


Figure 2. Calculated structures of (a) $\text{Fe}^{3+} \rightarrow \text{ACN}$; (b) $\text{Mg}^{2+} \rightarrow \text{ACN}$; (c) $\text{Sn}^{2+} \rightarrow \text{ACN}$.

For accomplishing a stable structure of $\text{Mg}^{2+} \rightarrow \text{ACN}$, $\text{Al}^{3+} \rightarrow \text{ACN}$, $\text{Ga}^{3+} \rightarrow \text{ACN}$, $\text{Sn}^{2+} \rightarrow \text{ACN}$, $\text{Cr}^{3+} \rightarrow \text{ACN}$, and $\text{Fe}^{3+} \rightarrow \text{ACN}$, a geometry optimization plus frequency calculations were done. Then, Bader charge and thermodynamic attributes of $\text{Al}^{3+} \rightarrow \text{ACN}$ chelation of Cya, Del, and Pet pigments owing to their B ring in gas and aqueous media at 300K were estimated in a periodic box of H_2O molecules (**Figure 3**). The optimized geometries include the bond length of “oxygen— $\text{Mg}^{2+} \approx (1.9\text{\AA})$ ” and the bond angle of “oxygen— Mg^{2+} —oxygen $\approx (112^\circ)$ ” “while it was found the bond length of oxygen— $\text{M}^{3+} \approx (1.8\text{\AA})$ and bond angle of oxygen— M^{3+} —oxygen $\approx (120^\circ)$ for trivalent metal ions of Al^{3+} , Cr^{3+} and Fe^{3+} (**Figure 3**).

The “Becke, 3-parameter, Lee-Yang-Parr (B3LYP) “hybrid density functional has been applied for years and it is proposed that the B3LYP method with the optimized semiempirical parameters can walk to be a good density functional in the computations of thermodynamic properties and reactivity of huge organic structures [46]. B3LYP is a hybrid functional, often applied to gain the bond lengths and vibrational frequencies near lab experiments amounts [47].

Our computations have been carried out due to the conceptual density functional theory (DFT)/B3LYP/6-31G (d,p) method using the projector– augmented–wave (PAW) methodology [48]. DFT is a method to solve the Schrödinger equation for the movements of electrons in structures based on the significance that the energy is a functional of the density. This approach is used in electronic structure calculations to both molecules and solids [49].

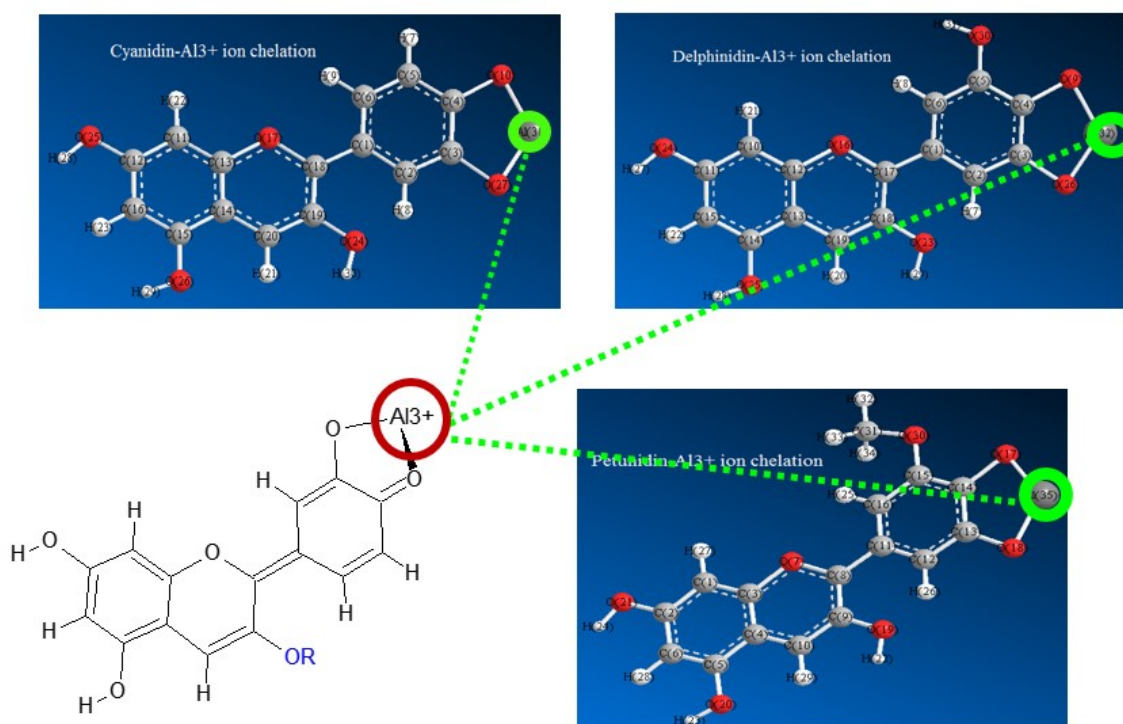


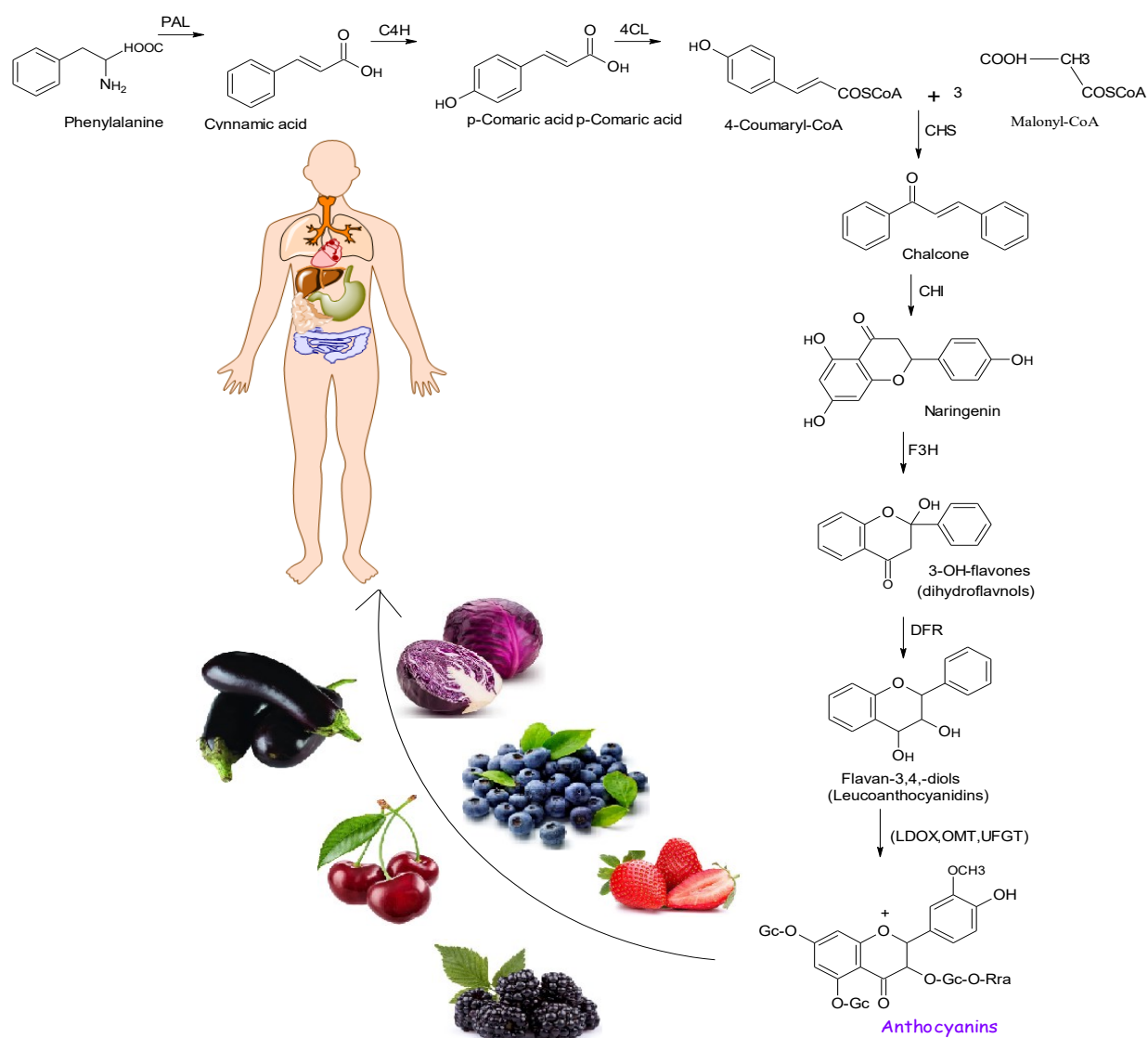
Figure 3. The schematics of optimized ACN—Al³⁺ ion chelation calculated by theoretical methods.

The theoretical computations have been run to attain more valid equilibrium geometrical data and infrared spectral information for each of the recognized complexes. The simulated model has been exhibited the theoretical methods which generate a current sample of a model at an identified temperature by measuring physicochemical specifications owing to the partition function.

3. Results and discussion

Phenolic plant seems to have multiple mechanisms of action in combating cancer including angiogenesis denying tumors vascular supply required for proliferation, inhibiting DNA synthesis, inducing apoptosis, and cellular differentiation inhibiting cancer progression [50, 51]. Regular consumption of raspberry ACNs is also reported to improve cognitive brain functions, age-related degeneration of eyesight and influence cardiovascular disease [52]. **Scheme 2** shows that ACNs are synthesized from precursors by two biosynthetic pathways.

For example, the blooms of wild raspberry with the color depending on the soil pH are reflected by Al³⁺ to the plant under acidic conditions while Al³⁺ changes the color of the ACN pigment. The thermodynamic properties for conjunction of “Mal, Peo, Del, Pet, Cya” with cations of “Mg²⁺, Al³⁺, Ga³⁺, Sn²⁺, Cr³⁺, Fe³⁺” in different pH has been measured using Gaussian 16 revision C.01 program in aqueous medium (**Table 1**).



Scheme 2. The Biosynthesis of ACN compounds.

Table 1. The Thermochemical specifications for “Cya, Del, Mal, Pel, Peo, Pet” in aqueous medium.

pigment	$\Delta G \times 10^{-5}$	$\Delta H \times 10^{-3}$	$\Delta S \times 10^{-2}$	$E_{\text{electronic}} \times 10^{-6}$	$E_{\text{core-core}} \times 10^{-6}$	$\ln K \times 10^{-5}$
Cya	-2.85	-1.54	9.44	-2.80	2.51	2.85
Del	-2.92	-1.57	9.69	-2.89	2.60	4.90
Mal	-2.11	-9.07	7.00	-1.86	1.65	3.54
Pel	-2.45	-1.26	8.14	-2.25	2.01	1.37
Peo	-2.72	-1.42	9.03	-2.61	2.33	4.56
Pet	-2.80	-1.47	9.28	-2.75	2.47	4.69

The difference of ΔH_f among the chelated complexes of $Mg^{2+} \rightarrow ACN$, $Al^{3+} \rightarrow ACN$, $Ga^{3+} \rightarrow ACN$, $Sn^{2+} \rightarrow ACN$, $Cr^{3+} \rightarrow ACN$, and $Fe^{3+} \rightarrow ACN$ (**Figure 3**) has been observed. The consequences of ΔH_f for “[Mg^{2+} , Al^{3+} , Ga^{3+} , Sn^{2+} , Cr^{3+} , $Fe^{3+} \rightarrow Cya, Del, Pet$]” complexes have been shown by **Figure 4** and reported data in **Table 1**.

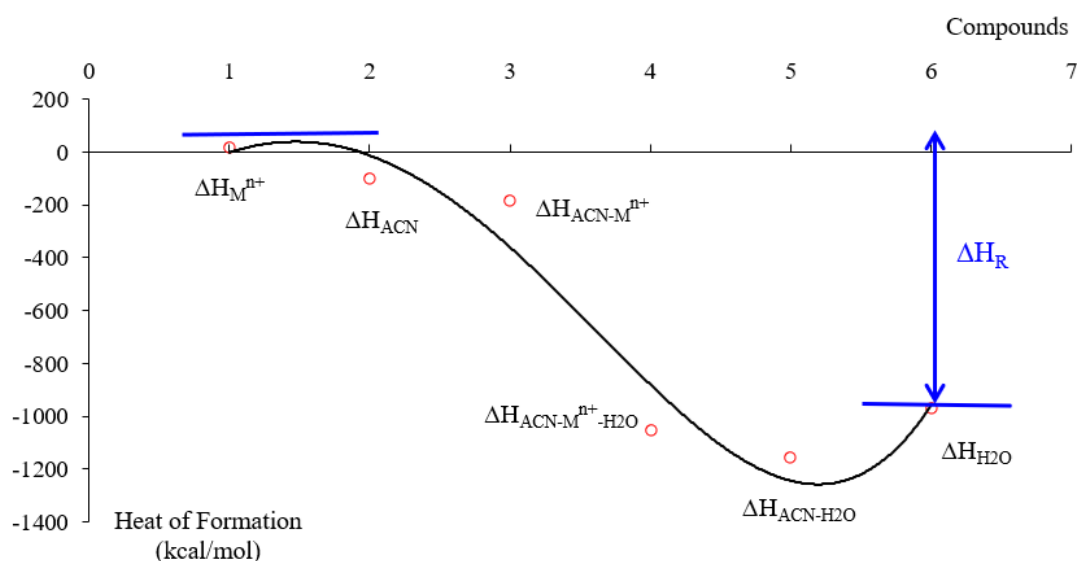


Figure 4. Enthalpy of reaction (ΔH_R) for formation of “ $Mg^{2+} \rightarrow ACN$, $Al^{3+} \rightarrow ACN$, $Ga^{3+} \rightarrow ACN$, $Sn^{2+} \rightarrow ACN$, $Cr^{3+} \rightarrow ACN$, and $Fe^{3+} \rightarrow ACN$ ” complexes.

The absorbance (A) of chelated cations including Mg^{2+} , Ga^{3+} , Cr^{3+} , Fe^{3+} , and Al^{3+} with Cya, Del, and Pet pigments in aqueous periodic box has been calculated (Table 2). The data have been shown based on equation of $A = \log_{10} (I_0/I) = \epsilon lc$, where A is the absorbance; I, intensity of current; ϵ , molar absorptivity coefficient and c, concentration of solution (Table 2).

Table 2. Measured “absorbance (A)”, “Frequency” and “Dipole moment” of metal \rightarrow ACN chelation of “Cya, Del, Pet” in various pH.

pH	$Mg^{2+} \times 10^{-3}$			$Ga^{3+} \times 10^{-3}$			$Cr^{3+} \times 10^{-3}$			$Fe^{3+} \times 10^{-3}$			$Al^{3+} \times 10^{-3}$					
	A	Frequency	Dipole	A	Frequency	Dipole	A	Frequency	Dipole	A	Frequency	Dipole	A	Frequency	Dipole			
1.17	0.10	3.922	3.05	0.25	3.925	18.65	0.22	3.926	9.94	0.13	3.925	0.25	0.25	3.924	18.65			
1.30	1.20	3.927	3.24	1.32	3.925	16.74	0.96	3.931	8.39	1.06	3.926	1.32	1.32	3.925	16.74			
1.40	1.21	3.927	1.53	0.64	3.926	16.35	0.65	3.926	10.31	0.95	3.926	0.64	0.64	3.926	16.35			
1.48	1.89	4.014	5.27	1.87	4.008	13.82	0.68	3.926	8.59	1.19	3.928	1.87	1.87	4.008	13.82			
1.54	1.89	4.012	3.91	1.85	4.007	6.69	1.90	4.009	9.59	1.90	4.012	1.85	1.85	4.007	6.69			
pH	Del			$Mg^{2+} \times 10^{-3}$			$Ga^{3+} \times 10^{-3}$			$Cr^{3+} \times 10^{-3}$			$Fe^{3+} \times 10^{-3}$			$Al^{3+} \times 10^{-3}$		
	A	Frequency	Dipole	A	Frequency	Dipole	A	Frequency	Dipole	A	Frequency	Dipole	A	Frequency	Dipole			
1.17	0.70	3.926	6.71	0.42	3.925	18.78	0.89	3.933	9.04	0.89	3.767	7.90	3.59	3.925	16.19			
1.30	1.20	3.929	3.67	1.25	3.927	14.94	0.89	3.933	9.04	3.93	3.945	7.47	1.07	3.929	17.15			
1.40	2.81	5.816	2.60	1.24	3.928	12.99	1.07	3.935	6.40	0.89	3.928	6.87	1.12	3.929	16.10			
1.48	1.24	3.930	4.91	3.75	4.041	15.99	1.92	4.018	7.38	1.92	4.018	5.54	1.86	4.015	17.01			
1.54	1.92	4.018	3.75	1.90	4.014	13.14	1.84	4.015	9.03	1.95	4.016	6.38	1.80	4.013	16.86			

Table 2. (Continued).

pH	Pet			Ga ³⁺ × 10 ⁻³			Cr ³⁺ × 10 ⁻³			Fe ³⁺ × 10 ⁻³			Al ³⁺ × 10 ⁻³		
	A	Frequency	Dipole	A	Frequency	Dipole	A	Frequency	Dipole	A	Frequency	Dipole	A	Frequency	Dipole
1.2	0.39	3.925	8.2	0.61	3.926	17.77	1.47	3.767	26.67	0.39	3.925	8.2	1.22	3.764	17.84
1.30	3.59	3.925	7.89	0.57	3.926	16.37	0.27	3.926	9.77	3.59	3.925	7.89	3.59	3.930	16.22
1.40	0.97	3.938	6.59	1.04	3.936	15.78	1.02	3.945	9.34	0.97	3.938	6.59	8.50	7.744	19.27
1.48	0.96	3.941	5.34	1.07	3.935	17.38	0.86	3.940	6.89	0.96	3.941	5.34	1.06	3.954	16.27
1.54	1.00	3.940	6.52	1.89	4.014	12.82	0.92	3.943	6.21	1.00	3.941	6.52	1.96	4.013	15.92

The reduction in absorbance might be related to reduced solubility of $M^{n+} \rightarrow$ ACN complexes which eventuate in precipitation of some complexes (**Figure 5a,b**). Furthermore, the complexes of $Ga^{3+} \rightarrow$ Pet, $Cr^{3+} \rightarrow$ Pet, $Mg^{2+} \rightarrow$ Pet (**Figure 5a**) and $Al^{3+} \rightarrow$ Cya, $Ga^{3+} \rightarrow$ Cya, $Mg^{2+} \rightarrow$ Cya (**Figure 5b**) have indicated the maximum absorbance in the low concentration.

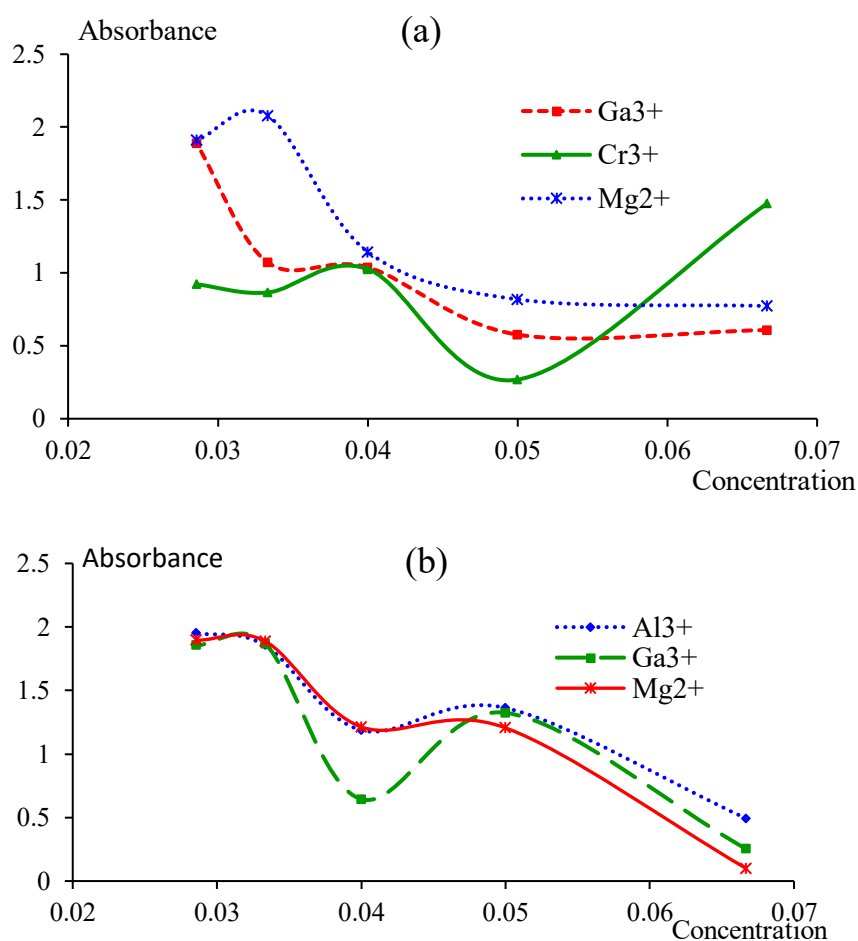


Figure 5. The graphs of Absorbance versus concentration for complexes of **(a)** $Ga^{3+} \rightarrow$ Pet, $Cr^{3+} \rightarrow$ Pet, $Mg^{2+} \rightarrow$ Pet; **(b)** $Al^{3+} \rightarrow$ Cya, $Ga^{3+} \rightarrow$ Cya, $Mg^{2+} \rightarrow$ Cya.

In computations, Al^{3+} was identified to displace Mg^{2+} in $\text{Mg}^{2+} \rightarrow \text{ACN}$ complexes, Cya based and produces more stable complexes (**Figure 6**).

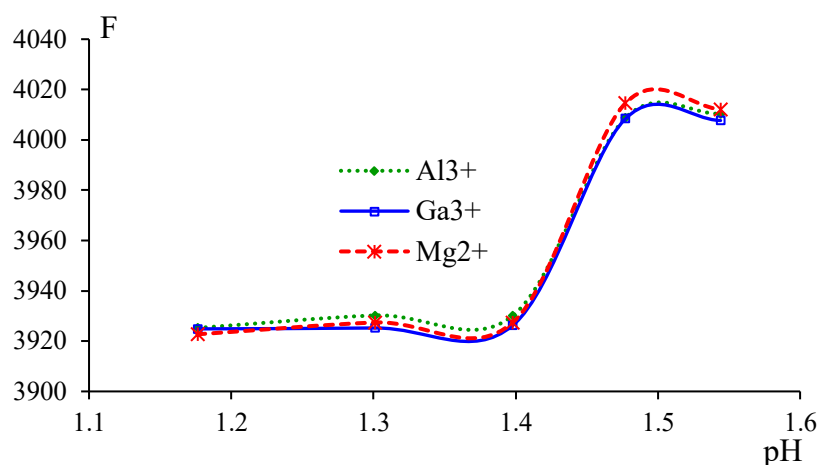


Figure 6. Fluctuation of frequency (F) versus pH for $\text{Al}^{3+} \rightarrow \text{Cya}$, $\text{Ga}^{3+} \rightarrow \text{Cya}$, $\text{Mg}^{2+} \rightarrow \text{Cya}$ complexes.

It has been seen that by increasing the pH, the frequency of $\text{Al}^{3+} \rightarrow \text{Cya}$, $\text{Ga}^{3+} \rightarrow \text{Cya}$, $\text{Mg}^{2+} \rightarrow \text{Cya}$ complexes increase between $\text{pH} \approx 1.1$ – 1.5 . The maximum frequency for $\text{Al}^{3+} \rightarrow \text{Cya}$, $\text{Ga}^{3+} \rightarrow \text{Cya}$, $\text{Mg}^{2+} \rightarrow \text{Cya}$ complexes is in the pH between 1.50 to 1.55 of weak acidic medium (**Figure 6**). Then, the “Bader charge” of indicated atoms in $\text{Mg}^{2+} \rightarrow \text{ACN}$, $\text{Ga}^{3+} \rightarrow \text{ACN}$, $\text{Cr}^{3+} \rightarrow \text{ACN}$, $\text{Fe}^{3+} \rightarrow \text{ACN}$, and $\text{Al}^{3+} \rightarrow \text{ACN}$ chelation has been measured as the active zones of the structures which represent a significant function for the “electron charge” transfer towards generating a range of different colors in aqueous medium (**Table 3**).

Table 3. The “Bader charge” for some particles of $\text{Mg}^{2+} \rightarrow \text{ACN}$, $\text{Ga}^{3+} \rightarrow \text{ACN}$, $\text{Cr}^{3+} \rightarrow \text{ACN}$, $\text{Fe}^{3+} \rightarrow \text{ACN}$, and $\text{Al}^{3+} \rightarrow \text{ACN}$ in aqueous medium.

Cyanidin					
Atom	Mg^{2+}	Ga^{3+}	Cr^{3+}	Fe^{3+}	Al^{3+}
O (10)	-0.42	-0.37	-0.02	-0.16	-0.36
O ⁺ (17)	-0.13	-0.16	-0.13	-0.14	-0.13
O (24)	-0.20	-0.23	-0.21	-0.21	-0.18
O (25)	-0.22	-0.22	-0.21	-0.22	-0.21
O (26)	-0.21	-0.21	-0.21	-0.21	-0.21
O (27)	-0.39	-0.34	0.07	-0.13	-0.33
M ⁿ⁺ (31)	0.76	0.76	-0.45	0.07	-0.02
Delphinidin					
Atom	Mg^{2+}	Ga^{3+}	Cr^{3+}	Fe^{3+}	Al^{3+}
O (9)	-0.39	-0.56	0.00	-0.14	-0.32
O ⁺ (16)	-0.13	-0.13	-0.13	-0.13	-0.13
O (23)	-0.20	-0.18	-0.21	-0.20	-0.18
O (24)	-0.21	-0.20	-0.20	-0.21	-0.20
O (25)	-0.21	-0.21	-0.21	-0.21	-0.21

Table 3. (Continued).

Cyanidin					
Atom	Mg ²⁺	Ga ³⁺	Cr ³⁺	Fe ³⁺	Al ³⁺
O (26)	-0.40	-0.63	0.06	-0.12	-0.33
O (30)	-0.21	-0.18	-0.21	-0.21	-0.19
M ⁿ⁺ (32)	0.76	0.64	-0.42	0.04	0.04
Petunidin					
Atom	Mg ²⁺	Ga ³⁺	Cr ³⁺	Fe ³⁺	Al ³⁺
O ⁺ (7)	-0.13	-0.13	-0.13	-0.13	-0.13
O (17)	-0.40	-0.57	0.03	-0.13	-0.33
O (18)	-0.39	-0.63	0.04	-0.17	-0.33
O (19)	-0.20	-0.19	-0.21	-0.21	-0.19
O (20)	-0.21	-0.19	-0.21	-0.20	-0.21
O (21)	-0.22	-0.21	-0.22	-0.22	-0.21
O (30)	-0.15	-0.12	-0.15	-0.15	-0.13
M ⁿ⁺ (35)	0.76	0.65	-0.42	0.0	0.03

The IR vibrational frequencies have shown that the “normal mode” of the active zones owing to cations → ACN chelation of “Al³⁺ → Cya, Al³⁺ → Del, and Al³⁺ → Pet”. The alteration of Bader charge for functionalized atoms through optimized complexes of Mg²⁺ → ACN, Al³⁺ → ACN, Ga³⁺ → ACN, Sn²⁺ → ACN, Cr³⁺ → ACN, and Fe³⁺ → ACN have been plotted in **Figure 7**.

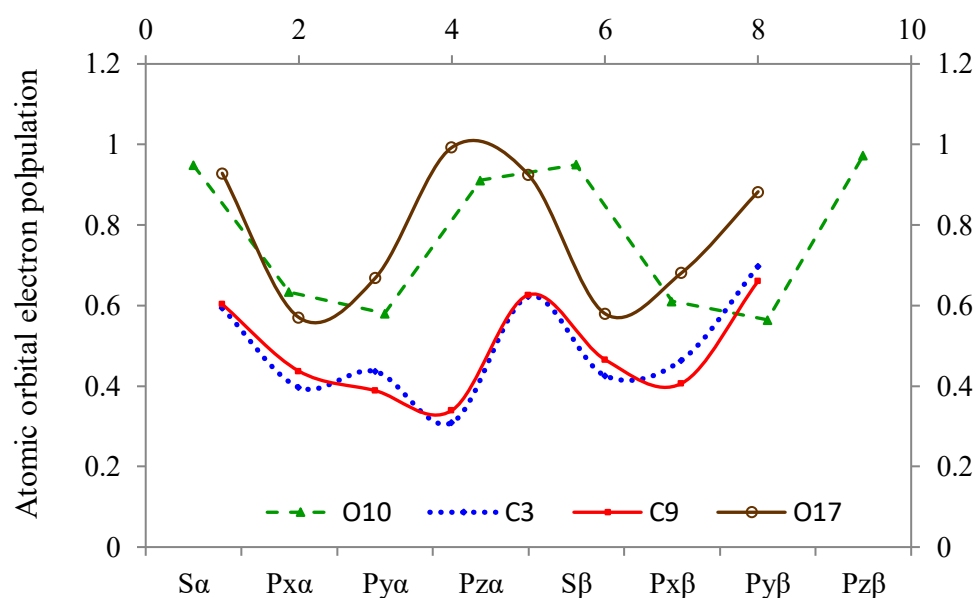


Figure 7. Atomic orbital electron population for some atoms through optimized Mg²⁺ → ACN, Al³⁺ → ACN, Ga³⁺ → ACN, Sn²⁺ → ACN, Cr³⁺ → ACN, and Fe³⁺ → ACN chelation in aqueous medium.

Thus, the electrophilic groups of Cya, Del ACN pigments lead us to explore the cause for the activity and the stability of these compounds in natural products. The perspective of **Figure 7** suggests the cause for observing a variety of consequences for

chelated complexes of “ $\text{Mg}^{2+} \rightarrow \text{ACN}$, $\text{Al}^{3+} \rightarrow \text{ACN}$, $\text{Ga}^{3+} \rightarrow \text{ACN}$, $\text{Sn}^{2+} \rightarrow \text{ACN}$, $\text{Cr}^{3+} \rightarrow \text{ACN}$, and $\text{Fe}^{3+} \rightarrow \text{ACN}$ ”.

The results are proposed to summarize the ACNs induced by different cations, mainly including Mg^{2+} , Al^{3+} , Ga^{3+} , Sn^{2+} , Cr^{3+} , Fe^{3+} . This chelation leads to the formation of a complex compound of ACN -cations. The mechanism of cation-induced ACNs mainly depends on the location of active zones of functionalized O-atoms in ACN and divalent or trivalent cations characteristics.

4. Conclusions

Applying beer-lambert proof on chelated complexes of $\text{Mg}^{2+} \rightarrow \text{ACN}$, $\text{Al}^{3+} \rightarrow \text{ACN}$, $\text{Ga}^{3+} \rightarrow \text{ACN}$, $\text{Sn}^{2+} \rightarrow \text{ACN}$, $\text{Cr}^{3+} \rightarrow \text{ACN}$, and $\text{Fe}^{3+} \rightarrow \text{ACN}$ using theoretical approaches indicates absorbance factor in gas and aqueous media and then explores the stabilization energy, thermodynamic specifications and the electronic structural of optimized cluster chelated of $\text{Mg}^{2+} \rightarrow \text{ACN}$, $\text{Al}^{3+} \rightarrow \text{ACN}$, $\text{Ga}^{3+} \rightarrow \text{ACN}$, $\text{Sn}^{2+} \rightarrow \text{ACN}$, $\text{Cr}^{3+} \rightarrow \text{ACN}$, and $\text{Fe}^{3+} \rightarrow \text{ACN}$. In addition, it has been discovered that $[(\text{Mg}^{2+}$, Al^{3+} , Ga^{3+} , Sn^{2+} , Cr^{3+} and $\text{Fe}^{3+}) \rightarrow \text{ACN}]$ cluster chelation is related to the axes of active areas of functionalized oxygen atoms and cations in these complexes which alter the electronic charges in aromatic cyclic chains because of aqueous dielectric constant compared to gas medium. Regarding the received results, regular consumption of some vegetables and fruits could be useful to monitor and inhibit COVID-19 disease by suppression of propagation and pathogenicity of SARS-CoV-2. Therefore, this research can collate all the possible mechanisms behind the behavior of cations (Mg^{2+} , Al^{3+} , Ga^{3+} , Sn^{2+} , Cr^{3+} and Fe^{3+}) in the cell as a drug at viral disease conditions through molecular modelling approaches and DFT framework.

Author contributions: Conceptualization, FM; methodology, FM and MM; software, FM and MM; validation, FM; formal analysis, FM and MM; investigation, FM and MM; resources, MM; data curation, FM and MM; writing—original draft preparation, FM; writing—review and editing, MM; visualization, FM and MM; supervision, FM; project administration, FM. All authors have read and agreed to the published version of the manuscript.

Acknowledgments: In successfully completing this paper and its research, the authors are grateful to Kastamonu University.

Ethical approval: Not applicable.

Conflict of interest: The authors declare no conflict of interest.

References

1. Alomair L, Mustafa S, Jafri MS, et al. Molecular Dynamics Simulations to Decipher the Role of Phosphorylation of SARS-CoV-2 Nonstructural Proteins (nsps) in Viral Replication. *Viruses*. 2022; 14(11): 2436. doi: 10.3390/v14112436
2. Zadeh MAA, Lari H, Kharghanian L, et al. Density Functional Theory Study and Anti-Cancer Properties of Shyshaq Plant: In View Point of Nano Biotechnology. *Journal of Computational and Theoretical Nanoscience*. 2015; 12(11): 4358-4367. doi: 10.1166/jctn.2015.4366
3. Monajjemi M, Afsharnezhad S, Jaafari MR, Mirdamadi S, Mollaamin F, Monajemi H, Investigation of energy and NMR isotropic shift on the internal rotation Barrier of Θ_4 dihedral angle of the DLPC: A GIAO study. *Chemistry*. 2008; 17(1): 55-69.

4. Monajjemi M, Mollaamin F, Shojaei S, An overview on coronaviruses family from past to COVID-19: Introduce some inhibitors as antiviruses from Gillan's plants. 2020; 10(3): 5575-5585. doi: 10.33263/BRIAC103.575585
5. Shahriari S, Monajjemi M, Mollaamin F. DETERMINATION OF PROTEINS SPECIFICATION WITH SARS- COVID-19 BASED LIGAND DESIGNING. *Journal of the Chilean Chemical Society*. 2022; 67(2): 5468-5476. doi: 10.4067/s0717-97072022000205468
6. Majeed A, Zhang X. On the Adoption of Modern Technologies to Fight the COVID-19 Pandemic: A Technical Synthesis of Latest Developments. *COVID*. 2023; 3(1): 90-123. doi: 10.3390/covid3010006
7. Mollaamin F. Conocimiento de enfermedades virales terapéuticas: aplicación de SWCNT en la administración de fármacos. *Revista Colombiana de Química*. Published online April 10, 2024: 28-35. doi: 10.15446/rev.colomb.quim.v52n2.111888
8. Mollaamin F. Characterizing the structural and physicochemical properties of medicinal plants as a proposal for treating of viral malady. *Trends in Immunotherapy*. 2023; 7(2): 2329. doi: 10.24294/ti.v7.i2.2329
9. Mollaamin F, Monajjemi M. THERMODYNAMIC RESEARCH ON THE INHIBITORS OF CORONAVIRUS THROUGH DRUG DELIVERY METHOD. *Journal of the Chilean Chemical Society*. 2021; 66(2): 5195-5205. doi: 10.4067/s0717-97072021000205195
10. Tahan A, Mollaamin F, Monajjemi M. Thermochemistry and NBO analysis of peptide bond: Investigation of basis sets and binding energy. *Russ. J. Phys. ChemA*, 2009; 83(4): 587-597. doi: 10.1134/S003602440904013X
11. Mollaamin F. Structural and Functional Characterization of Medicinal Plants as Selective Antibodies towards Therapy of COVID-19 Symptoms. *Antibodies*. 2024; 13(2): 38. doi: 10.3390/antib13020038
12. Zeng F, Huang Y, Guo Y, et al. Association of inflammatory markers with the severity of COVID-19: A meta-analysis. *International Journal of Infectious Diseases*. 2020; 96: 467-474. doi: 10.1016/j.ijid.2020.05.055
13. Mollaamin F. PHYSICOCHEMICAL INVESTIGATION OF ANTI-COVID19 DRUGS USING SEVERAL MEDICINAL PLANTS. *Journal of the Chilean Chemical Society*. 2022; 67(2): 5537-5546. doi: 10.4067/s0717-97072022000205537
14. Jamal QMS. Antiviral Potential of Plants against COVID-19 during Outbreaks—An Update. *International Journal of Molecular Sciences*. 2022; 23(21): 13564. doi: 10.3390/ijms232113564
15. Remali J, Aizat WM. A Review on Plant Bioactive Compounds and Their Modes of Action Against Coronavirus Infection. *Frontiers in Pharmacology*. 2021; 11. doi: 10.3389/fphar.2020.589044
16. Mollaamin F, Shahriari S, Monajjemi M. MONKEYPOX DISEASE TREATMENT BY TECOVIRIMAT ADSORBED ONTO SINGLE-WALLED CARBON NANOTUBE THROUGH DRUG DELIVERY METHOD. *Journal of the Chilean Chemical Society*. 2023; 68(1): 5796-5801. doi: 10.4067/s0717-97072023000105796
17. Capell T, Twyman RM, Armario-Najera V, et al. Potential Applications of Plant Biotechnology against SARS-CoV-2. *Trends in Plant Science*. 2020; 25(7): 635-643. doi: 10.1016/j.tplants.2020.04.009
18. Mollaamin F, Monajjemi M. B5N10 Nanocarrier Functionalized with Al, C, Si Atoms: A Drug Delivery Method for Infectious Disease Remedy. *OBM Genetics*. 2024; 08(01): 1-19. doi: 10.21926/obm.genet.2401214
19. Murugesan S, Ragavendran C, Ali A, et al. Screening and Druggability Analysis of Marine Active Metabolites against SARS-CoV-2: An Integrative Computational Approach. *International Journal of Translational Medicine*. 2022; 3(1): 27-41. doi: 10.3390/ijtm3010003
20. Castro-Acosta ML, Lenihan-Geels GN, Corpe CP, et al. Berries and anthocyanins: promising functional food ingredients with postprandial glycaemia-lowering effects. *Proceedings of the Nutrition Society*. 2016; 75(3): 342-355. doi: 10.1017/s0029665116000240
21. Paredes-López O, Cervantes-Ceja ML, Vigna-Pérez M, et al. Berries: Improving Human Health and Healthy Aging, and Promoting Quality Life—A Review. *Plant Foods for Human Nutrition*. 2010; 65(3): 299-308. doi: 10.1007/s11130-010-0177-1
22. Mollaamin F, Monajjemi M. Drug delivery using doping of boron nitride nanosensor towards releasing chloroquine drug in the cells: A promising method for overcoming viral disease. *Rev. Colomb. Cienc. Quím. Farm.*, 2024; 53(2): 430-454. <https://doi.org/10.15446/rcciquifa.v53n2.114450>
23. Torres PHM, Sodero ACR, Jofily P, et al. Key Topics in Molecular Docking for Drug Design. *International Journal of Molecular Sciences*. 2019; 20(18): 4574. doi: 10.3390/ijms20184574
24. Das S, Sarmah S, Lyndem S, et al. An investigation into the identification of potential inhibitors of SARS-CoV-2 main protease using molecular docking study. *Journal of Biomolecular Structure and Dynamics*. Published online May 13, 2020: 1-11. doi: 10.1080/07391102.2020.1763201

25. Monajjemi M, Sobhanmanesh A, Mollaamin F, Theoretical studies of solvent effects on binding of Sn (CH₃)₂(N-acetyl-L-cysteinate) with single-walled carbon nanotube. Fuller. Nanotub. Carbon Nanostructures. 201; 21(1): 47-63. doi: 10.1080/1536383X.2011.574325
26. Mpiana PT, Ngbolua K te N, Tshibangu DST, et al. Identification of potential inhibitors of SARS-CoV-2 main protease from Aloe vera compounds: A molecular docking study. Chemical Physics Letters. 2020; 754: 137751. doi: 10.1016/j.cplett.2020.137751
27. Khalili Hadad B, Mollaamin F, Monajjemi M. Biophysical chemistry of macrocycles for drug delivery: a theoretical study. Russian Chemical Bulletin. 2011; 60(2): 238-241. doi: 10.1007/s11172-011-0039-5
28. Mollaamin F, Monajjemi M. THERMODYNAMIC RESEARCH ON THE INHIBITORS OF CORONAVIRUS THROUGH DRUG DELIVERY METHOD. Journal of the Chilean Chemical Society. 2021; 66(2): 5195-5205. doi: 10.4067/s0717-97072021000205195
29. Mazzini S, Musso L, Dallavalle S, et al. Putative SARS-CoV-2 Mpro Inhibitors from an In-House Library of Natural and Nature-Inspired Products: A Virtual Screening and Molecular Docking Study. Molecules. 2020; 25(16): 3745. doi: 10.3390/molecules25163745
30. Mollaamin F, Monajjemi M. MOLECULAR DRUG DISCOVERY OF POTENTIAL INHIBITOR OF COVID-19 USING SEVERAL MEDICINAL PLANT INGREDIENTS: A PROMISING THERAPY FOR VIRAL DISEASE. Revista de la Facultad de Ciencias. 2024; 13(1): 141-158. doi: 10.15446/rev.fac.cienc.v13n1.111288
31. Alfaro M, Alfaro I, Angel C. Identification of potential inhibitors of SARS-CoV-2 papain-like protease from tropane alkaloids from Schizanthus porrigens: A molecular docking study. Chemical Physics Letters. 2020; 761: 138068. doi: 10.1016/j.cplett.2020.138068
32. Mollaamin F. Computational Methods in the Drug Delivery of Carbon Nanocarriers onto Several Compounds in Sarraceniaceae Medicinal Plant as Monkeypox Therapy. Computation. 2023; 11(4):84. doi: 10.3390/computation11040084
33. Olsson ME, Gustavsson KE, Andersson S, et al. Inhibition of Cancer Cell Proliferation in Vitro by Fruit and Berry Extracts and Correlations with Antioxidant Levels. Journal of Agricultural and Food Chemistry. 2004; 52(24): 7264-7271. doi: 10.1021/jf030479p
34. Mollaamin F, Monajjemi M. Application of DFT/TD-DFT Frameworks in the Drug Delivery Mechanism: Investigation of Chelated Bisphosphonate with Transition Metal Cations in Bone Treatment. Chemistry. 2023; 5(1):365-380. doi: 10.3390/chemistry5010027
35. Ghalandari B, Monajjemi M, Mollaamin F. Theoretical investigation of carbon nanotube binding to DNA in view of drug delivery. J Comput Theor Nanosci. 2011; 8(7): 1212-1219. doi:10.1166/jctn.2011.1801
36. Mollaamin F, Shahriari S, Monajjemi M, TREATING OMICRON BA.4 & BA.5 VIA HERBAL ANTIOXIDANT ASAFOETIDA: A DFT STUDY OF CARBON NANOCARRIER IN DRUG DELIVERY. J. Chil. Chem. Soc. 2023; 68(1): 5781-5786. doi: 10.4067/S0717-97072023000105781
37. Sarasia EM, Afsharnezhad S, Honarparvar B, et al. Theoretical study of solvent effect on NMR shielding tensors of luciferin derivatives. Physics and Chemistry of Liquids. 2011; 49(5): 561-571. doi: 10.1080/00319101003698992
38. Mollaamin F. Computational Methods in the Drug Delivery of Carbon Nanocarriers onto Several Compounds in Sarraceniaceae Medicinal Plant as Monkeypox Therapy. Computation. 2023; 11(4): 84. doi: 10.3390/computation11040084
39. Monajjemi M, Yamola H, Mollaamin F, Study of bio-nano interaction outlook of amino acids on single-walled carbon nanotubes. Fuller. Nanotub. Carbon Nanostructures. 2014; 22(6): 595-603. doi: 10.1080/1536383X.2012.702163
40. Schreiber HD, Swink AM, Godsey TD. The chemical mechanism for Al³⁺ complexing with delphinidin: A model for the bluing of hydrangea sepals. Journal of Inorganic Biochemistry. 2010; 104(7): 732-739. doi: 10.1016/j.jinorgbio.2010.03.006
41. Schreiber HD, Swink AM, Godsey TD. The chemical mechanism for Al³⁺ complexing with delphinidin: A model for the bluing of hydrangea sepals. Journal of Inorganic Biochemistry. 2010; 104(7): 732-739. doi: 10.1016/j.jinorgbio.2010.03.006
42. Mollaamin F, Shahriari S, Monajjemi M. Therapeutic role of medicinal plants against viral diseases focusing on COVID-19: Application of computational chemistry towards drug design. Rev. Colomb. Cienc. Quím. Farm., 2024; 53(1): 19-43. <https://doi.org/10.15446/rcciquifa.v53n1.112978>
43. Chitrala KN, Yang X, Busbee B, et al. Computational prediction and in vitro validation of VEGFR1 as a novel protein target for 2,3,7,8-tetrachlorodibenzo-p-dioxin. Scientific Reports. 2019; 9(1). doi: 10.1038/s41598-019-43232-4

44. Mollaamin F, Shahriari S, Monajjemi M. DRUG DESIGN OF MEDICINAL PLANTS AS A TREATMENT OFOMICRON VARIANT (COVID-19 VARIANT B.1.1.529). *Journal of the Chilean Chemical Society*. 2022; 67(3): 5562-5570. doi: 10.4067/s0717-97072022000305562
45. Frisch MJ. Trucks GW. Schlegel HB. Scuseria GE. Robb MA. Cheeseman JR. et al. Gaussian 16, Revision C.01, Gaussian, Inc., Wallingford CT, 2016.
46. Becke AD. Density-functional thermochemistry. III. The role of exact exchange. *The Journal of Chemical Physics*. 1993; 98(7): 5648-5652. doi: 10.1063/1.464913
47. Perdew JP, Ernzerhof M, Burke K. Rationale for mixing exact exchange with density functional approximations. *The Journal of Chemical Physics*. 1996; 105(22): 9982-9985. doi: 10.1063/1.472933
48. Mollaamin F, Monajjemi M, Molecular modelling framework of metal-organic clusters for conserving surfaces: Langmuir sorption through the TD-DFT/ONIOM approach. *Molecular Simulation*, 2023; 49(4): 365-376. doi: 10.1080/08927022.2022.2159996
49. White WM, ed. *Encyclopedia of Geochemistry*. Springer International Publishing; 2018. doi: 10.1007/978-3-319-39312-4
50. Marko D, Puppel N, Tjaden Z, et al. The substitution pattern of anthocyanidins affects different cellular signaling cascades regulating cell proliferation. *Molecular Nutrition & Food Research*. 2004; 48(4): 318-325. doi: 10.1002/mnfr.200400034
51. Katsube N, Iwashita K, Tsushida T, et al. Induction of Apoptosis in Cancer Cells by Bilberry (*Vaccinium myrtillus*) and the Anthocyanins. *Journal of Agricultural and Food Chemistry*. 2002; 51(1): 68-75. doi: 10.1021/jf025781x
52. Zafra-Stone S, Yasmin T, Bagchi M, et al. Berry anthocyanins as novel antioxidants in human health and disease prevention. *Molecular Nutrition & Food Research*. 2007; 51(6): 675-683. doi: 10.1002/mnfr.200700002